Organic Electronics 13 (2012) 705–709

Contents lists available at SciVerse ScienceDirect

Organic Electronics

journal homepage: www.elsevier.com/locate/orgel

Highly efficient inverted rapid-drying blade-coated organic solar cells

Jung-Hao Chang [a], Yi-Hong Chen [a], Hao-Wu Lin [a,*], Yu-Ting Lin [a], Hsin-Fei Meng [b], En-Chen Chen [c]

[a] Department of Materials Science and Engineering, National Tsing Hua University, Hsinchu 300, Taiwan
[b] Institute of Physics, National Chiao Tung University, Hsinchu 300, Taiwan
[c] Department of Electrical Engineering, National Tsing Hua University, Hsinchu 300, Taiwan

ARTICLE INFO

Article history:
Received 27 September 2011
Received in revised form 27 November 2011
Accepted 31 December 2011
Available online 29 January 2012

Keywords:
Inverted organic solar cells
Blade coating
Bulk hetero-junction

ABSTRACT

Efficient inverted bulk-heterojunction (BHJ) poly(3-hexylthiophene):[6,6]-phenyl C61 butyric acid methyl ester (P3HT:PCBM) organic solar cells fabricated by rapid-drying blade-coated were demonstrated. Optimized self-organization interpenetration networks and donor/acceptor domain sizes were obtained while maintaining the smooth surface morphology. By integrating with low-temperature-processed sol–gel ZnO electron extraction layer, power conversion efficiency (PCE) up to 4.4% under AM1.5G 1 sun illumination is achieved, compared to fast drying but low efficiency (1.2%) and high efficiency but with long-time solvent annealing treatment (4.3%) control cells deposited by spin coating in chlorobenzene (CB) and 1,2-dichlorobenzene (DCB) solution, respectively. The novel deposition technique reveals a promising process for highly efficient, high throughput, stable morphology organic solar cells fabrication.

1. Introduction

In the past decade, BHJ organic solar cells (OSCs) based on mixture of conjugated polymers and fullerene derivatives have attracted great interests due to their potential as low-cost, large-area, and light weight renewable energy sources. In the conventional OSCs, active organic materials are sandwiched between anode buffer layer poly(3,4-ethylenedioxythiophene):poly(styrene sulfonate) (PEDOT:PSS) and low-work-function metal cathode (e.g., Al, Ca). It has been reported that these devices exhibit poor stabilities due to hygroscopic and acidic nature of PEDOT:PSS and reactivity of low-work-function metal [1,2]. In order to overcome these problems, OSCs with the inverted structure which utilize low-reactivity metals (e.g., Ag) for anode and metal oxides (e.g., ZnO, TiO_2) for electron extraction at the cathode have been developed [3–10].

It has been notice that the organic active layer morphologies to device efficiencies are significant influenced by different deposition techniques and treatments [11,12]. Nowadays, the spin-coating is the most widely used to fabricate OSCs. However, the advanced coating technologies which are compatible to roll-to-roll mass production such as spray coating [13–15], screen printing [16], gravure printing [17], ink-jet printing [18] and blade coating [19–21] have been under development. Nevertheless, all the part of the published work so far has been done in conventional non-inverted structure which is not ideal device configuration for long-term stability. Moreover, hours of solvent or thermal annealing was needed to increase materials crystallinity and larger phase separation domains for efficient carrier transportation.

In this study, we show that in the case of P3HT:PCBM BHJ, the morphology formation for the rapid-drying blade-coated process is fundamentally different to the film forming by spin-coated. Unique morphology with large phase separation domains were formed instantaneously while maintaining very smooth surface. By carefully integrating the blade-coated active layer with metal oxide charge extraction layers, PCE up to 4.4% was obtained. The results demonstrate the benefits of fabrication inverted

* Corresponding author.
E-mail address: hwlin@mx.nthu.edu.tw (H.-W. Lin).

1566-1199/$ - see front matter © 2012 Elsevier B.V. All rights reserved.
doi:10.1016/j.orgel.2011.12.025

OSCs with rapid-drying blade-coated for optimized interpenetration carrier pathway, high PCE and smooth surface morphology.

2. Experimental

2.1. Device fabrication

The schematics of the device structure and band diagram in this study are shown in Fig. 1. Indium tin oxide (ITO) coated glass substrates (sheet resistance ~15 Ω/sq) were cleaned in an ultrasonic bath with de-ionized water, acetone, and methanol for 15 min, respectively. The sol–gel films of ZnO (~4 nm, measured by ellipsometer) were spin coated of a zinc acetate [Zn(ac)] solution (7.3 g/l) in 96% 2-methoxy ethanol and 4% ethanolamine onto pre-cleaned ITO-coated glass substrates [22]. The ZnO sol–gel films were then annealed in air at 150 °C for 5 min. A blend solution of P3HT (17 mg ml^{-1}, purchased from Rieke Metals) and PCBM (17 mg ml^{-1}, purchased from Nano-C) was prepared using CB or DCB as solvents. Three kinds of active layers were prepared: Device A, A2: P3HT:PCBM was prepared in CB (Device A) and DCB (Device A2) solution and was blade-coated on the ZnO-coated ITO substrate. In order to achieve rapid-drying the substrate was kept at 100 °C for solvent evaporation, the films were dried instantaneously within few seconds, no additional solvent annealing was performed in these devices. Device B, D: P3HT:PCBM was prepared in CB (Device B) and DCB (Device D) solution and was spin-coated on the ZnO-coated ITO substrate, no additional solvent annealing was performed in these devices. Device C: P3HT:PCBM was prepared in DCB solution and was spin-coated on the ZnO-coated ITO substrate, the films were slow-dried (solvent-annealed) in a closed glass vial for 8 h. The P3HT:PCBM active layer thicknesses were controlled by spinning speed (spin-coated) or gap from blade to substrate (blade-coated) and kept ~200 nm for all the samples in this study. After the coating of organic active layers, devices A, A2, B, C, D were annealed at 140 °C for 5 min to further stabilize the morphology, the performance of devices do not change after and before annealed process. Then the samples were transferred to vacuum chamber (base pressure ~1×10^{-6} Torr) for hole extraction layers and metal electrodes deposition. All the transfer processes were done in inert atmosphere without exposure to air. All devices in this study were with the same structure: ITO(150 nm)/ZnO(4 nm)/P3HT:PCBM (200 nm, various deposition condition)/MoO_3(20 nm)/Ag(120 nm). The active area of the cells had an average size of 5 mm^2. Devices were encapsulated using a UV-cured sealant (*Everwide Chemical Co., Epowide EX*) and a cover glass under the dry nitrogen atmosphere after fabrication and were measured in air.

2.2. Device characterization

Current density–voltage characteristics of solar cells were measured with a SourceMeter *Keithley* 2636A under illumination of AM1.5G solar light from a solar simulator

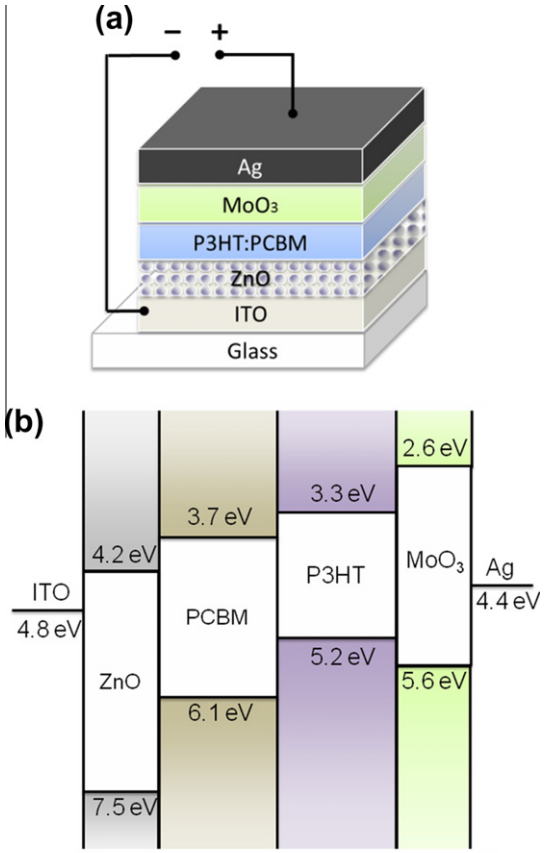

Fig. 1. (a) Device structure and (b) energy level diagram of the inverted organic solar cells in this study.

(*Abet Technologies*). The incident light intensity was calibrated as 100 mW/cm^2. The external quantum efficiency (EQE) spectra were taken by illuminating chopped monochromatic light with a continuous-wave bias white light (from halogen lamp, intensity ~100 mW/cm^2) on the solar cells. The photocurrent signals were extracted with lock-in technique using a current preamplifier (*Stanford Research System*) followed by a lock-in amplifier (*AMETEK*). The EQE measurement is fully computer controlled and the intensity of monochromatic light is carefully calibrated with optical power meter (*Ophir Optronics*). Organic films for absorption spectroscopy and ellipsometry measurements were deposited on fused silica substrates. Absorption spectra were acquired with *PerkinElmer* spectrometer and ellipsometry measurements were carried out with *J. A. Woollam Inc. V-VASE* variable-angle spectroscopic ellipsometer. Atomic force microscopy (AFM) images were taken with *Veeco Nanoscope 3100* atomic force microscope. The X-ray diffraction (XRD) measurement was carried out using a TTRAX III (Rigaku, Japan) diffractometer equipped with a rotating anode Cu target (wavelength, $\lambda = 0.154$ nm). The film preparation conditions for the AFM and XRD measurements were kept the same as device fabrication for accurate comparison.

3. Results and discussion

Fig. 2 shows the current density–voltage characteristics of OSCs and Table 1 shows the open-circuit voltage (V_{OC}), short-circuit current (J_{sc}), fill factor (FF) and power conversion efficiency (PCE) of each cells. Interestingly, the CB solvent, rapid-drying blade-coated Device A and the DCB solvent with long-time solvent annealed, spin-coated Device C show comparable efficiencies up to 4.4% and 4.3%, respectively, while the CB solvent, spin-coated Device B spin-coated cells without solvent annealed shows much lower efficiency of 1.2%. Note that by change from the fabrication method of traditional spin-coating to blade-coating, while keep the device structure and layers thicknesses in the same condition, the V_{OC}, J_{sc} and FF all increase largely (Device A vs. Device B). Only when spin-coated samples were exerted with long time solvent annealing could achieve comparable performance of rapid-drying blade-coated samples (Device A vs. Device C). This observation was double confirmed by fabrication and measurements of DCB solvent, spin-coated cells without long-time solvent annealing (Device D, see Supporting Information). Even with high boiling-point DCB solvent, the spin-coated cells without long-time solvent annealing could only show 2.6% PCE, which still much lower than efficiency of Device A. The results indicate that the blend layer morphologies and charge carrier percolation networks were extensively affected by process method.

The difference in J_{sc} between three cells (Device A, B and C) is also reflected in the external quantum efficiency spectra shown in Fig. 3. Device A and B, which dissolve P3HT:PCBM in the same CB solvent show EQE spectra with similar shape. However, the maximum EQE of blade-coated device approaches impressive ~89% value compare

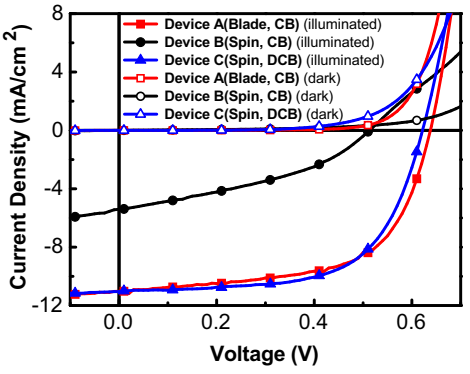

Fig. 2. *J–V* characteristics of Device A (Blade-coated, in CB solution) (square), Device B (Spin-coated, in CB solution) (circle) and Device C (Spin-coated, in DCB solution) (triangle).

Table 1
The performance of organic solar cells in this work.

	V_{OC} (V)	J_{SC} (mA/cm^2)	FF (%)	PCE (%)
Device A (Blade, CB)	0.65	10.9	62	4.4
Device B (Spin, CB)	0.52	6.0	39	1.2
Device C (Spin, DCB)	0.62	11.0	63	4.3

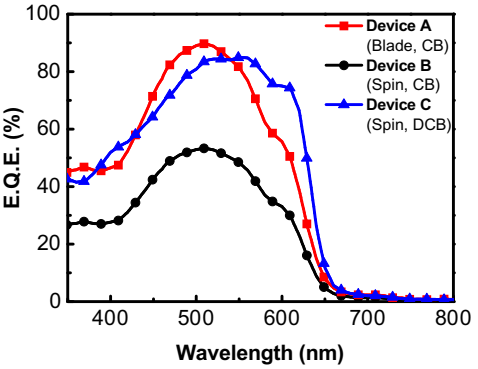

Fig. 3. External quantum efficiency spectra of Device A (Blade-coated, in CB solution) (square), Device B (Spin-coated, in CB solution) (circle) and Device C (Spin-coated, in DCB solution) (triangle).

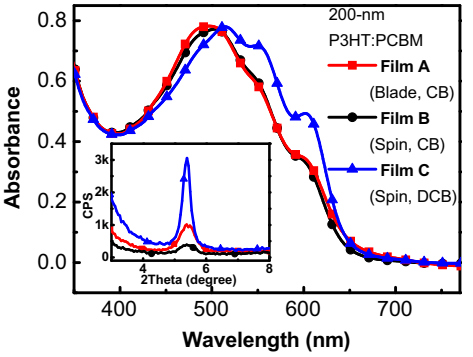

Fig. 4. Absorption spectra and (inset) XRD patterns of CB solution, blade-coated (square), CB solution, spin-coated (circle) and DCB solution, spin-coated (triangle) P3HT:PCBM thin-film.

to only ~50% in spin-coated device. On the other hand, the device prepare in DCB solvent shows red-shifted EQE spectrum with fully developed shoulders in the 585–625 nm wavelength range, which can also be observed in DCB solvent without solvent-annealing Device D (see Supporting Information). The higher EQE value of Device C around 600 nm may be contributed by higher crystallinity of P3HT with 8-h solvent annealing, which was revealed in XRD signals shown in inset of Fig. 4 [23].

To investigate whether the apparent higher quantum efficiency in rapid-drying blade-coated device then in spin-coated device is due to higher photon absorption or lower carrier recombination, UV–Vis spectroscopy was performed on 200-nm thin films on the fused silica substrate. The preparation conditions for the absorption measurements were kept the same as device fabrication for accurate comparison. The results are shown in Fig. 4. The shapes of absorption spectra clear reflect the shape of EQE spectra. The 200-nm P3HT:PCBM thin-film prepared in CB solution shows almost identical absorption spectra with max absorbance ~0.83 and thin-film prepared in DCB solution shows red-shifted absorption spectrum with max absorbance also ~0.83. The results clearly indicate that the amount of photon absorption is almost identical

in Device A and B. However, in Device A, due to the optimum carrier transporting passageways are formed, higher EQE values were observed, while in Device B, the carrier transport is blocked and higher carrier recombination rate results in lower quantum efficiency.

The interpretation of device performance of different fabrication condition can also be supported by tapping-mode AFM images as shown in Fig. 5. The phase images of rapid-drying blade-coated, CB solvent P3HT:PCBM thin-film (Fig. 5(b)) and spin-coated with solvent annealing, DCB solvent P3HT:PCBM thin-film (Fig. 5(f)) show well-developed donor/acceptor segregation with domain size ~20 nm. On the contrary, the donor/acceptor separation is undistinguish in spin-coated, CB-solution P3HT:PCBM thin-film with domain size less than 10 nm. However, as shown in inset of Fig. 4, the P3HT crystallization signals of P3HT:PCBM thin-film are (Spin, DCB) ≫ (Blade, CB) ⩾ (Spin, CB), indicates that the larger domain size of DCB-solution thin-film is caused by high crystallinity of solvent-annealed P3HT, but the larger domain size of blade-coated thin film is due to spontaneous formation of donor/acceptor segregation when blading the thin film [12,24]. The clear donor/acceptor networks result in a large interfacial area for efficient charge generation and continuous pathways for carrier transport.

Surface morphologies of the thin-films are shown in Fig. 5(a), (c), and (e) and the roughness characteristics are listed in Table 2. The films made from low-boiling-point

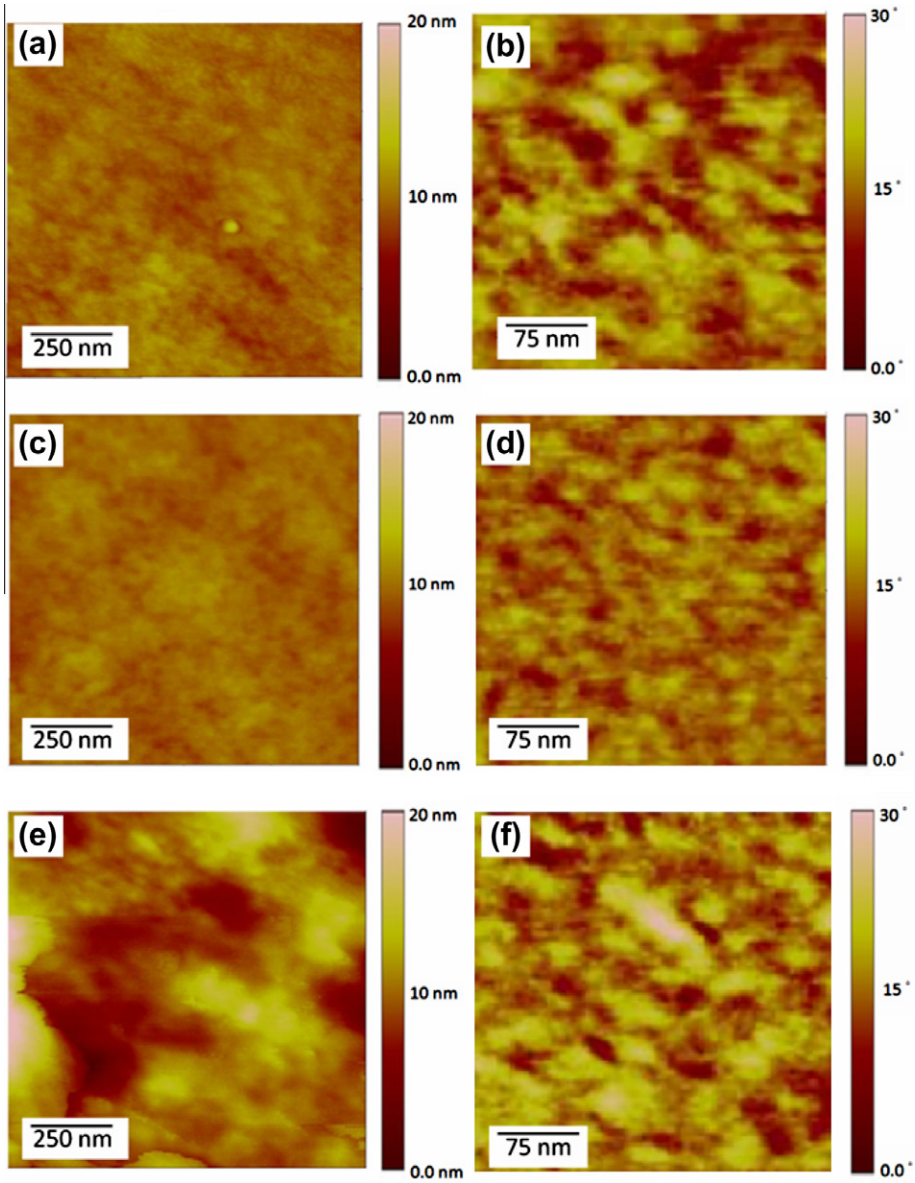

Fig. 5. AFM topology (left) and phase (right) images of (a and b) CB solution, blade-coated P3HT:PCBM thin-film, (c and d) CB solution, spin-coated P3HT:PCBM thin-film and (e and f) DCB solution, spin-coated P3HT:PCBM thin-film. The thin-films were prepared on low-temperature sol–gel ZnO coated ITO substrates.

Table 2
Surface roughness characteristics of the P3HT:PCBM thin-film.

	R_{rms} (nm)	R_a (nm)	R_{max} (nm)
Device A (Blade, CB)	0.74	0.58	7.61
Device B (Spin, CB)	0.59	0.46	4.43
Device C (Spin, DCB)	2.69	2.00	21.32

CB solvent show very smooth surface with the root-mean-square (rms) roughness of 0.59–0.74 nm, regardless the deposition methods. On the other hand, inevitable high roughness of rms roughness of 2.69 nm and maximum roughness of more than 21 nm were shown in the films with long time solvent annealing (crystal development, see inset of Fig. 4) process.

4. Conclusions

In summary, the rapid-drying blade-coated P3HT:PCBM thin-films show intriguing properties of smooth morphology and spontaneous donor/acceptor material segregation. Compare to the traditional spin-coated method, which high-boiling point-solvent-annealing technique is needed to achieve similar phase separation, the blade coating method create competitive interpenetrated carrier passageways with smoother surface and much shorter process time (1–2 s) present in both CB and DCB solvent (Device performance of blade-coated device fabricated with DCB solvent was shown in Supporting Information). By integrating the rapid-drying blade-coated active layer with low-temperature sol–gel ZnO electron extraction layer and thermal evaporated MoO_3 hole extraction layer, high efficiency OSCs are demonstrated with PCE of ~4.4%. With these encouraging results and the compatibility of roll-to-roll process [25], one envisage that rapid-drying blade-coated technique may provide a new promising way of high-efficiency, high-stability and high-throughput organic solar cells fabrication.

Acknowledgements

We thank the National Science Council of Taiwan (NSC 98-2112-M-007-028-MY3) and the Low Carbon Energy Research Center, National Tsing-Hua University, for financial support.

Appendix A. Supplementary data

Supplementary data associated with this article can be found, in the online version, at doi:10.1016/j.orgel. 2011. 12.025.

References

[1] M. Jørgensen, K. Norrman, F.C. Krebs, Sol. Energy Mater. Sol. Cells 92 (2008) 686.
[2] K. Norrman, S.A. Gevorgyan, F.C. Krebs, ACS Appl. Mater. Interf. 4 (2009) 102.
[3] S.K. Hau, H.L. Yip, N.S. Baek, J. Zou, K. O'Malley, A.D.Y. Jen, Appl. Phys. Lett. 92 (2008) 253301.
[4] Y. Sun, J.H. Seo, C.J. Takacs, J. Seifter, Alan J. Heeger, Adv. Mater. 23 (2011) 1679.
[5] C. Waldauf, M. Morana, P. Denk, P. Schilinsky, K. Coakley, S.A. Choulis, C.J. Brabec, Appl. Phys. Lett. 89 (2006) 233517.
[6] J.C. Wang, C.Y. Lu, J.L. Hsu, M.K. Lee, Y.R. Hong, T.P. Perng, S.F. Horng, H.F. Meng, J. Mater. Chem. 21 (2011) 5723.
[7] Y. Jouane, S. Colis, G. Schmerber, P. Kern, A. Dinia, T. Heisera, Y.A. Chapuis, J. Mater. Chem. 21 (2011) 1953.
[8] S. Schumann, R.D. Campo, B. Illy, A.C. Cruickshank, M.A. McLachlan, M.P. Ryan, D.J. Riley, D.W. McComb, T.S. Jones, J. Mater. Chem. 21 (2011) 2381.
[9] J.P. Liu, K.L. Choy, X.H. Hou, J. Mater. Chem. 21 (2011) 1966.
[10] J.C. Wang, W.T. Weng, M.Y. Tsai, M.K. Lee, S.F. Horng, T.P. Perng, C.C. Kei, C.C. Yu, H.F. Meng, J. Mater. Chem. 20 (2010) 862.
[11] M. Hirade, H. Nakanotani, M. Yahiro, C. Adachi, Appl. Mater. Interf. 3 (2011) 80.
[12] G. Li, V. Shrotriya, J. Huang, Y. Yao, T. Moriarty, K. Emery, Y. Yang, Nat. Mater. 4 (2005) 864.
[13] C. Girotto, D. Moia, B.P. Rand, P. Heremans, Adv. Funct. Mater. 21 (2011) 64.
[14] C. Girotto, B.P. Rand, J. Genoe, P. Heremans, Sol. Energy Mater. Sol. Cells 93 (2009) 454.
[15] J.S. Kim, W.S. Chung, K. Kim, D.Y. Kim, K.J. Paeng, S.M. Jo, S.Y. Jang, Adv. Funct. Mater. 20 (2010) 3538.
[16] S.E. Shaheen, R. Radspinner, N. Peyghambarian, G.E. Jabbour, Appl. Phys. Lett. 79 (2001) 18.
[17] P. Kopola, T. Aernouts, S. Guillerez, H. Jin, M. Tuomikoski, A. Maaninen, J. Hast, Sol. Energy Mater. Sol. Cells 94 (2010) 1673.
[18] C.N. Hoth, P. Schilinsky, S.A. Choulis, C.J. Brabec, Nano Lett. 8 (2008) 9.
[19] Y.H. Chang, S.R. Tseng, C.Y. Chen, H.F. Meng, E.C. Chen, S.F. Horng, C.S. Hsu, Org. Electron. 10 (2009) 741.
[20] W.B. Byun, S.K. Lee, J.C. Lee, S.J. Moon, W.S. Shin, Curr. Appl. Phys. 11 (2011) S179.
[21] P. Schilinsky, C. Waldauf, C.J. Brabec, Adv. Funct. Mater. 16 (2006) 1669.
[22] W.J.E. Beek, M.M. Wienk, M. Kemerink, X. Yang, R.A.J. Janssen, J. Phys. Chem. B 109 (2005) 9505.
[23] P. Vanlaeke, G. Vanhoyland, T. Aernouts, D. Cheyns, C. Deibel, J. Manca, P. Heremans, J. Poortmans, Thin Solid Films 511 (2006) 358.
[24] W. Ma, C. Yang, X. Gong, K. Lee, A.J. Heeger, Adv. Funct. Mater. 15 (2005) 1617.
[25] S.R. Tseng, H.F. Meng, K.C. Lee, S.F. Horng, Appl. Phys. Lett. 93 (2008) 153308.